A Supra-monolayer Nanopattern for Organic Nanoparticle Array Deposition
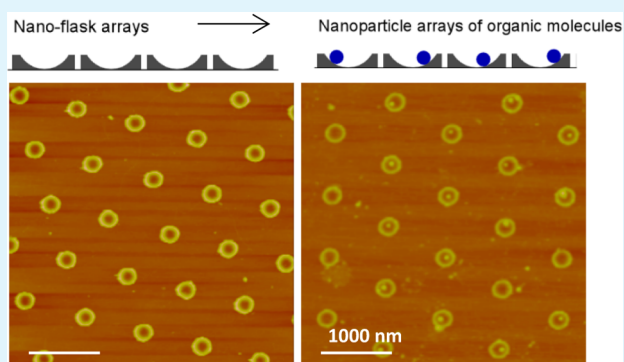
Sunxi Wang, Daniel J. Sobczynski, Pedram Jahanian, Juxhin Xhahysa, and Guangzhao Mao*

Department of Chemical Engineering and Materials Science, Wayne State University, 5050 Anthony Wayne Drive, Detroit, Michigan 48202, United States

ⓢ *Supporting Information*

ABSTRACT: Nanopatterns have applications in many areas including sensors, optoelectronics, and crystallization screening. Particle lithography is a convenient method to manufacture nanoring nanopatterns based on organosilane surface chemistry. The pattern thickness is generally limited to the monolayer thickness. This work is focused on the chemical vapor deposition conditions that yield nanopatterns with multilayer thickness. The supra-monolayer n-octadecyltrichlorosilane (OTS) nanoring patterns are made using polystyrene particle lithography. The supra-monolayer nanopatterns are used as "nano-flasks" to deposit and nucleate nanoparticles of small organic molecules including n-docosane, aspirin, and clarithromycin. The supra-monolayer OTS nanopattern is an effective template for

nanoparticle array deposition of all three chemicals with high degree of fidelity to the substrate pattern. The nanoparticle size is varied by solution concentration. The preferential deposition of the organic molecules inside the nanoring is attributed to the dewetting of the liquid film on the nanopattern. The dewetting process effectively distributes the liquid film among the "nano-flasks" so that millions of solution experiments can be carried out in isolated droplets with droplet volume as small as 1×10^{-10} nL. The research demonstrates a method to manufacture "nano-flask" arrays for high-throughput nanoparticle deposition trials and manufacture of monodisperse organic/drug nanoparticles through self-assembly.

KEYWORDS: *nanopattern, nanoparticle array, crystallization, nanoconfinement, AFM*

INTRODUCTION

The self-assembled monolayers (SAMs) of organosilanes including n-octadecyltrichlorosilane (OTS) on silicon substrates have been extensively studied because of their potential applications in sensors and electronics.[1−3] OTS molecules chemically adsorb on the substrate surface (silicon dioxide) through the Si−O−Si covalent bond. The stability of the SAMs is further improved by the Si−O−Si bond between neighboring surface-bound OTS molecules. The close-packed OTS monolayer has been characterized by ellipsometry, X-ray reflectivity, and contact angle goniometry to exhibit a thickness of 2.6 nm, molecular packing density about 21 Å^2/molecule, and water contact angle reaching 110°.[4,5] In our previous work,[3] we have obtained smoother OTS monolayers using chemical vapor deposition (CVD) while the OTS monolayers deposited from the liquid phase often contain molecular aggregates. The precise control of the CVD is however complicated by the role of water in the competitive condensation and polymerization reactions of the OTS. Trace water is necessary for organosilane condensation reaction with the hydroxyl groups at the silicon substrate; however, excessive water causes polymerization of the organosilane molecules that result in vertical growth of multilayer islands.[6,7]

Particle lithography (also known as nanosphere lithography) relies on immersion capillary force between monodisperse colloidal particles to produce films of colloidal crystals on solid substrates.[8,9] Two-stage mechanism of the colloidal array formation has been proposed. In the first nucleation stage, particles start to order due to the immersion capillary force when the thickness of the water layer is close to the particle diameter. In the second crystal growth stage, water evaporation from the menisci gives rise to a convective flux of particles toward the nucleus. The combination of the organosilane SAM and particle lithography has yielded a simple yet reliable method to manufacture nanoring patterns on silicon substrates.[10−12] Organosilanes including OTS and silanes with amine and poly(ethylene oxide) functional groups have been deposited as nanorings on oxidized silicon and mica substrates. The surface density and sizes of the organosilane nanorings can be simply varied by the colloidal particle size. The nanopattern morphology has been found to be sensitive to the drying conditions. It is conceivable that the organosilane nanopattern can be used as a new type of templates to regulate the

deposition of nanoparticle arrays of diverse materials in a similar way as demonstrated on other types of micropatterns and nanopatterns.[13−19] For example, calcite nanoparticles could be deposited on the organosilane nanoring pattern following a similar mechanism of calcite crystallization on micropatterns of alkanethiol SAMs.[13] Hydrophobic drug nanoparticles could be deposited on the organosilane nanoring pattern by utilizing the amphiphilic nanostructure of the substrate as demonstrated in aspirin deposition on self-assembled phospholipid nanopattern on the graphite substrate.[17]

This study explores the competitive nature of the surface condensation vs polymerization reaction of the OTS molecules on oxidized silicon substrates covered by the lithographical colloidal layers. Monodisperse polystyrene particles with diameters of 300 and 900 nm are used. We investigate the CVD conditions that favor the polymerization reaction in the interstitial space of the colloidal crystal, which results in the OTS supra-monolayer nanopattern with a thickness exceeding that of the predominant OTS monolayer nanopattern. The OTS supra-monolayer patterns are used as "nano-flasks" to induce area-selective precipitation and nucleation of small organic molecules including n-docosane, 2-acetoxybenzoic acid (i.e., aspirin), and clarithromycin. We demonstrate that nucleation and crystallization of small organic molecules such as 2-acetoxybenzoic acid and n-carboxylic acids are influenced by nanoconfinement imposed by nanopatterns[17,18,20] and nanoparticle nucleation seeds.[21−23] In this work n-docosane is chosen because it belongs to the n-alkane homologous series with well-defined chain length-dependent crystallization behavior. In addition to evaporative crystallization from the solution phase, n-docosane can be recrystallized from the melt phase at 43 °C, close to room temperature. 2-Acetoxybenzoic acid and clarithromycin are active pharmaceutical ingredients (APIs) that are crystalline in nature. Crystallization of the APIs at the nanoscale is relevant to drug formulation to improve bioavailability. The supra-monolayer OTS nanopattern is found to be an effective template for nanoparticle array deposition of all three chemicals with uniform particle size and spatial distribution as dictated by the OTS pattern size. The deposited particle size can be varied by the solution concentration. The research demonstrates a particle lithographical method that overcomes the pattern thickness limit of the organosilane SAM and its potential use for high-throughput crystallization trials. The solution-based particle array formation method can be scaled up for nanomanufacture of small-molecule nanoparticles of drugs, dyes, and semiconductors.

■ EXPERIMENTAL SECTION

Materials. The following chemicals have been used as received: n-octadecyltrichlorosilane (OTS, 95%, Gelest), hydrogen peroxide (30% in water, Fisher), sulfuric acid (98% in water, Fisher), sodium chloride (99%, Fisher), magnesium chloride (>99%, Fisher), potassium sulfate (>99%, Fisher), ethanol (200 proof, Fluka), chloroform (99.9%, Fisher), diethyl ether (>99%, Alfa Aesar), 1-butanol (99.9%, Fisher), heptane (99%, Fisher), n-docosane ($C_{22}H_{46}$, 99%, Aldrich), 2-acetoxybenzoic acid ($C_9H_8O_4$, > 99%, Sigma), clarithromycin ($C_{38}H_{69}NO_{13}$, > 95%, Sigma). Deionized water from the Barnstead Nanopure water purification system (electrical resistivity 18 MΩ cm) has been used.
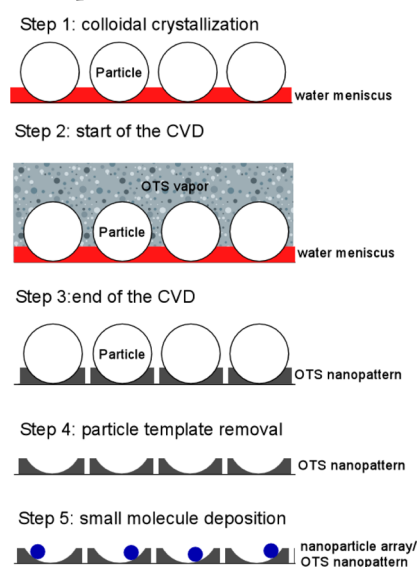
One-sided polished N type silicon (111) wafers (test grade, with resistivity of 1−20 Ω cm and thickness of 525 ± 50 μm) have been purchased from the Wafer World. Organic residues on the silicon wafer have been removed by immersing it in 3:1 mixture of sulfuric acid and 30% hydrogen peroxide for 1 h (*caution: this solution is highly

corrosive and needs to be handled with care!*). The substrate has been washed with copious amounts of deionized water and dried in stream of compressed N_2.

Particle Lithography. Monodisperse polystyrene microspheres with diameters of 900 nm (PS900) and 300 nm (PS300) have been used in particle lithography. Both have been purchased from the Thermo Scientific. The polystyrene particle suspension has been centrifuged for 15 min at 13,000 rpm (Thermo Scientific, Sorvall Legend XTR Centrifuge). The solid pellet at the bottom of the centrifuge tube has been redispersed in deionized water to a concentration of 1 w/v%. Approximately 30 μL of the suspension has been placed on a 1 × 1 cm² silicon wafer substrate for 30−45 min in the ambient laboratory atmosphere (relative humidity 40%) for colloidal crystallization. The substrate has been vacuum-dried for 30 min in order to remove excess water.

The stepwise procedure to create the OTS nanopattern and subsequent deposition of nanoparticles of small organic molecules is illustrated by Scheme 1. The OTS nanoring pattern on the polystyrene

Scheme 1. Side View of Steps That Lead to OTS Supra-monolayer Nanoring Formation (step 1−4) and Deposition of Small Molecule Nanoparticle Arrays on the OTS Nanopattern (step 5)

colloidal crystal template is conducted by modifying a literature procedure.[10−12] The polystyrene template is placed in a desiccator with 100 μL OTS. The desiccator is maintained at 70 °C for 90 min for the CVD. The relative humidity in the desiccator is varied by using saturated salt solutions and measured by a humidity meter (HX71-MA, Omega) immediately prior to the OTS reaction. Two desiccators are used. One is 0.13 L in volume and the other is 5.2 L. In both reactors, the sample, silane source, and humidity meter are placed close to each other with the sample placed 2 cm apart from the silane source and the humidity meter 1 cm apart from the sample. After the reaction, the polystyrene particles are removed by sonication (Bransonic, Ultrasonic Cleaner, 1510R-MTH) in a 1:1 mixture of ethanol and deionized water for 30−60 min to reveal the OTS nanorings.

Deposition of Small Organic Molecules on the OTS Nanoring Nanopattern. By trial and error, we have found that droplet solutions in the range of 40 μL are ideal for organic nanoparticle deposition on the 1 cm² OTS nanorings by evaporative recrystallization. Lower amount results in incomplete coverage of the substrate by the solution while higher amount results in thick deposits masking the nanorings. The droplet amount is further adjusted for each type of materials at different solution concentrations. In melt recrystallization of n-docosane, it is necessary to limit its amount

deposited on the substrate so that the nanoring pattern is not completely masked by the *n*-docosane layer. This has been achieved by evaporative deposition of sufficiently dilute *n*-docosane solution. The substrate covered by the *n*-docosane thin film is heated at 90 °C (above its melting temperature) for 30 min. The substrate is cooled immediately to −20 °C.

Characterization. The particle lithography and organic nanoparticle deposition are characterized by AFM and field-emission SEM (FESEM). AFM images are obtained with the J scanner (maximum scan area =125 × 125 μm^2) (Nanoscope IIIa, VEECO). Height, amplitude, and phase images are obtained in the tapping mode in ambient air. Uncoated silicon probes (TESP, VEECO) with a factory-specified spring constant of 40 N/m, length of 125 μm, width of 40 μm, and nominal tip radius of curvature less than 10 nm are used. The scan rate used is in the range of 0.5−1 Hz depending on the scan size. Integral and proportional gains are approximately 0.4 and 0.8, respectively. All reported AFM images are height images unless specified. Height images have been plane-fit in the fast scan direction with no additional filtering operation. Images are analyzed using the Nanoscope software from Digital Instruments (version 5.12). The various lateral and vertical sizes are measured manually using the sectional height analysis command. The nanoparticle volumes are measured by the bearing analysis command.

The nanostructures are characterized by a thermal FESEM (JEOL JSM-7600F). A thin layer of gold (∼10 nm) is sputter-coated (EffaCoater) on the sample for better image resolution. The FESEM images are obtained at a working distance of 8 nm and voltage of 15 kV.

The surface hydrophobicity is measured with an NRL contact angle goniometer (Model 100, Rame-Hart) in the laboratory atmosphere. A 10 μL water droplet is placed on the substrate and the static contact angles are measured on both sides of the droplet. Three droplets are placed at various spots on the substrate and the average readings are reported. The typical error is ±3°. The crystalline structure of 2-acetoxybenzoic acid nanoparticles is analyzed by FTIR (Perkin-Elmer Spectrum 400).

■ RESULTS AND DISCUSSION

Supra-Monolayer Nanopattern Formation by Particle Lithography. By following literature methods,[8,9] we are able to form large single-crystalline domains of polystyrene colloidal crystals on the oxidized silicon wafer. Figure 1 shows the colloidal layers formed by PS900 and PS300 particle lithography on the oxidized silicon wafer. The average single crystalline domain size is estimated to be 90 μm for the PS900 and 30 μm for the PS300. The SEM and AFM images show that more than one layer of polystyrene particles are deposited

though we find that the subsequent OTS pattern is templated only by the immediate interfacial particle layer on the substrate.

The silicon wafer substrates covered by the PS900 and PS300 colloidal layers are used as templates for OTS nanoring formation. The OTS nanorings are the result of surface hydrosilation initiated by nanoscopic amounts of water confined to the substrate by the colloidal particles.[10] We have produced both the expected monolayer pattern and the unexpected thicker pattern (referred here as the supra-monolayer pattern). Figure 2a, b shows the expected OTS nanorings made with the PS900 template. The high degree of order of the nanorings is shown by the intense fast Fourier transform (fft) of the AFM image. The nanopattern thickness is measured by AFM sectional height analysis to be 3.0 ± 0.5 nm (*N* = 50), which is consistent with the SAM structure of the
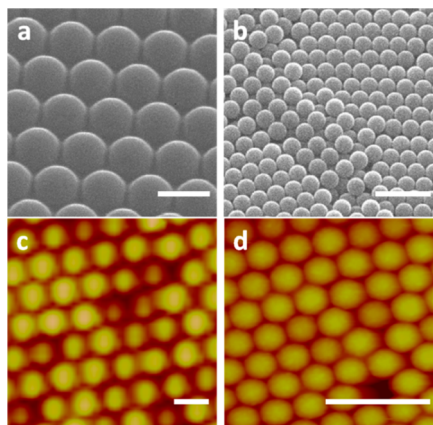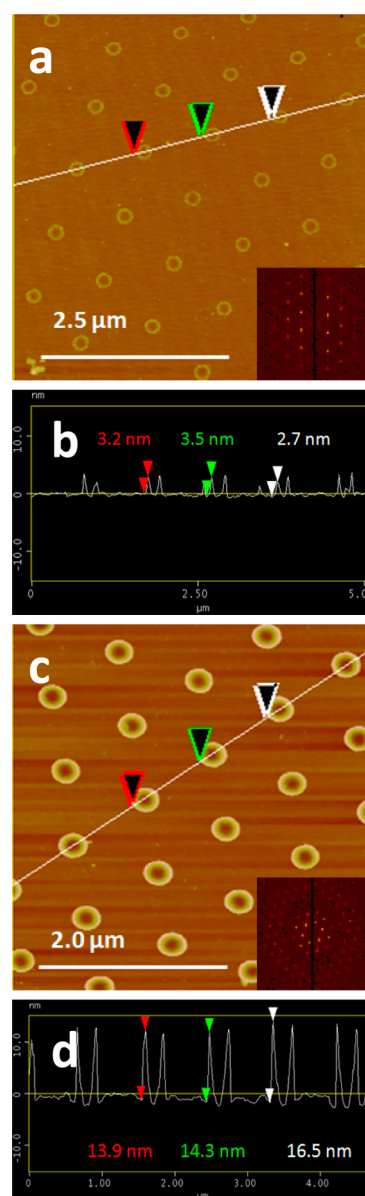

Figure 1. (a, b) SEM and (c, d) AFM height images (*z* range = 300 nm) of the (a, c) PS900 and (b, d) PS300 colloidal layers deposited on the oxidized silicon wafer. The bar length = 1 μm.

Figure 2. (a) AFM height image of the OTS monolayer nanorings and corresponding fft analysis (inset). Z-range = 30 nm. (b) The sectional height profile along the line in a. (c) AFM height image of OTS supra-monolayer nanorings and corresponding fft analysis (inset). Z-range = 60 nm. (d) The sectional height profile along the line in c.

OTS monolayer. In contrast, we have also observed OTS nanopatterns with thickness exceeding that of the OTS monolayer using the same particle templates but under different reaction conditions. Figure 2c, d shows an OTS supra-monolayer pattern with a pattern thickness of 14.4 ± 2.4 nm (N = 50) with the PS900 template. The reaction conditions that yield the supra-monolayer patterns are investigated and are the subject of the remaining report.

The OTS deposition on colloidal particle templates is studied as a function of reaction time, relative humidity, and reactor volume. The OTS amount is fixed at 100 μL. First, the reaction time is varied from 5 to 720 min at a relative humidity of 5% and temperature of 24 °C in the 0.13 L reactor. The OTS deposition is characterized by contact angle measurements and AFM. Figure 3 shows the water contact angle variation with the
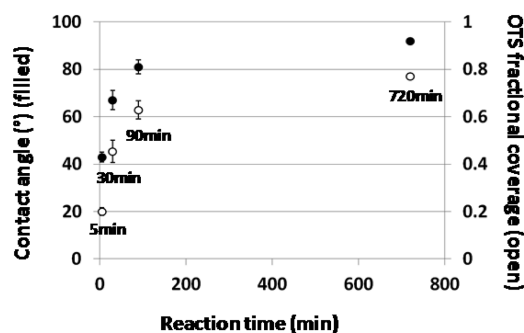
Figure 3. Contact angle and corresponding OTS fractional surface coverage on the oxidized silicon wafer as a function of the reaction time.

reaction time. The contact angle increases steadily during the initial 90 min of reaction and reaches a maximum value of 92° at 720 min. The OTS fractional area coverage (f) is estimated from the contact angle value (θ) using the Cassie equation (eq 1) assuming the Wenzel state[24] and is plotted in Figure 3

$$\cos \theta = f \cos \theta_{OTS} + (1 - f)\cos \theta_S \qquad (1)$$

θ_{OTS} and θ_S are the contact angles of the OTS monolayer and substrate (oxidized silicon wafer), which are assumed to be 110 and 0°, respectively.[25] The effect of surface roughness is neglected in this calculation. f is calculated to be 0.20 when $\theta = 43°$ at 5 min reaction time and 0.77 from when $\theta = 92°$. The actual f value can be determined from the AFM images. The f value in the PS900 case is determined to be 0.14 by counting an average of 24 OTS rings each with an outer diameter of 379 nm and inner diameter of 160 nm in a 4 × 4 μm^2 area (see Scheme S1a, Supporting Information). A closer look at the AFM sectional height profile of the nanorings shows a spherical cap bottom indicating various amounts of OTS deposited inside the ring tapering off toward the ring center (Figure 4a and Scheme S1b, Supporting Information). Taking into account the OTS deposition inside the ring by approximating the nanoring to a spherical disk (see Scheme S1c in the Supporting Information) with a disk diameter of 379 nm the f value is calculated to be 0.17. This is closer to the value based on the contact angle. Increasing amount of OTS is deposited outside the rings with increasing reaction time. Figure 4b shows the AFM data at 720 min reaction time. In contrast to the 5 min case (Figure 4a) there is a height difference between the area outside the ring and the bottom of the ring. The height difference, ~3 nm, closely matches the OTS monolayer thickness. Therefore one
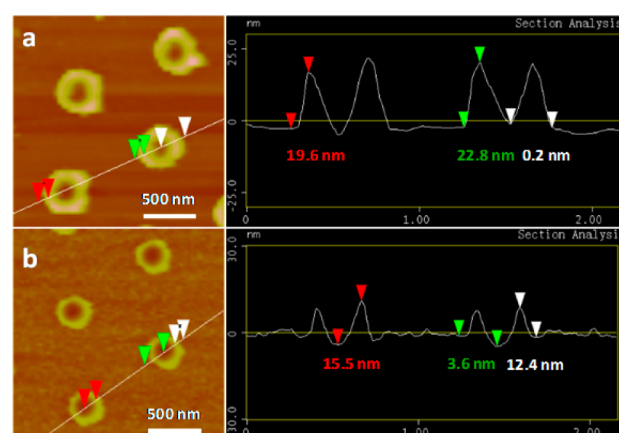
Figure 4. AFM height images of the OTS nanorings after 5 min reaction time (a) and 720 min reaction time (b) using the PS900 template. Z-range = 60 nm.

can conclude that the increase in contact angle is due to increasing OTS deposition outside the nanoring with reaction time to yield a hydrophobic nanoring nanopattern (see Scheme S1d in the Supporting Information).

The OTS nanopattern thickness varies between 14 and 23 nm with the maximum value reached at the beginning of the reaction (5 min). After reacting 30 min and longer the nanoring height remains at 14−17 nm. SEM has been used to examine the polystyrene particles removed from the substrate after being used as the template for OTS nanoring formation. Figure S1a (Supporting Information) shows the particles removed from the substrate by an adhesive tape as has been previously demonstrated by others.[26] The round patches of OTS film can be seen on top of the polystyrene particles. Figure S1b (Supporting Information) shows the remnants of the OTS film in the interstitial region among neighboring polystyrene particles when particles are sheared off the substrate by sonication. Some remnants are broken while others are still connected to the opposing polystyrene particles. This suggests that the top portion of the OTS nanorings may be broken off when the polystyrene particles are sheared off the substrate during the removal process. Such remnants are only observed after prolonged reaction suggesting the higher nanoring height at 5 min is probably due to weaker adhesion at the OTS film and polystyrene particle interface at the beginning of the reaction. It may be possible increase the nanopattern height by preventing tearing of the OTS nanopattern during removal of the polystyrene template.

Figure 5 plots the nanoring height as a function of relative humidity and reactor volume at 24 °C after 90 min of reaction time with a fixed OTS liquid volume of 100 μL. The relative humidity is varied from 5 to 39, 79, and 98% by N$_2$ purge and use of saturated MgCl$_2$, NaCl, and K$_2$SO$_4$ solution, respectively. Glass desiccators of volume 0.13 and 5.2 L are used as reactors. The data show that relative humidity has a weak effect on the nanopattern thickness. However, the supra-monolayer pattern only forms when the reactor volume is sufficiently small. The pattern thickness is around the monolayer thickness when the larger 5.2 L desiccator is used. The small reactor volume is necessary to maintain a sufficiently high OTS vapor pressure for bulk polymerization reaction confined to the interstitial space among the polystyrene particles. It may be possible to make thicker nanorings by methods to maintain high OTS vapor pressure near the sample surface.
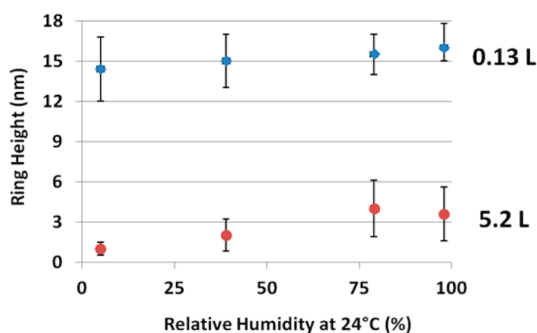
Figure 5. Nanoring height variation is plotted against the relative humidity in 5.2 and 0.13 L reactors. The PS900 template is used.

The SAMs of organosilanes including OTS on silicon substrates have been extensively studied.[1,2,27,28] The hydrolysis of the Si−Cl group to form the Si−OH bonds is initiated with trace amount of water. HCl is the byproduct. Then the silanol group reacts with the hydroxyl group on the oxidized silicon surface by condensation. H_2O is the byproduct. The remaining silanol groups can either react with unbound silanol groups from neighboring OTS molecules or the hydroxyl groups on the substrate in the absence of free silanol groups to yield the monolayer structure.[6,29,30] The outmost methyl group makes OTS monolayer hydrophobic (contact angle ≈ 110°). The close packing of OTS (∼ 21 Å^2/molecule) could be achieved by prolonged reaction time. Alternatively, the remaining silanol groups can polymerize with the silanol groups from unattached OTS molecules to form supra-monolayers (previously referred to by others as "multilayers").[6,7,31] Here we term these thicker films as supra-monolayers because there is no evidence that these films display a layered structure. Trichlorosilanes such as OTS has a tendency to polymerize among themselves.[32]

The supra-molecular OTS nanoring formation can be described based on silanol reactivity variation with different water structures in three zones as described in the literature.[33,34] Three zones of unique water structures have been identified in the particle lithographical template:[33] (1) cavity directly underneath the colloidal particle, (2) meniscus beyond the cavity area, and (3) free surface beyond the meniscus area. In Zone 1, ice-like water structures persist up to ≤10 nm in cavity diameter.[34] The ice-like water structure is characterized by anomalous changes in the density and surface tension of the water, which is attributed to the interaction of water molecules with surface hydroxyl groups on the oxidized silicon and hydrogen bond formation among water molecules.[34] Here the ice-like water structure is used to explain the limited reactivity of water in Zone 1. Our results of empty region with no OTS deposition fit the description of Zone 1. In Zone 1, the organosilane deposition is prevented by the steric hindrance imposed by the opposing solid substrates and surrounding liquid meniscus as well as low water reactivity. In Zone 2, water is assumed to liquefy due to capillary condensation. OTS condensation reaction with the surface hydroxyl groups occurs in the direction of the receding water contact line upon water evaporation. This yields the expected OTS monolayer pattern. However, our results show that there exists a competition between surface condensation to form the monolayer and polymerization to form the supra-monolayer in the meniscus zone. At low OTS concentration using the larger reactor volume the surface condensation dominates to yield the monolayer nanorings. At high OTS concentration using the smaller reactor volume the 3D polymerization reaction dominates to yield the supra-monolayer nanorings. Lastly in Zone 3, the free surface area is covered by planar ice-like water structures up to 3 molecular layers with or without a surface liquid layer depending on the relative humidity.[35] The ice-like water structure again hinders the OTS surface condensation reaction. In our case, the hydrophobic OTS nanopattern obtained only at longer reaction times is consistent with the notion that OTS surface condensation reaction occurs in Zone 3 at a slower reaction rate than that in Zone 2.

Supra-monolayer Nanorings Used for Organic Nano-particle Deposition. Next we explore the use of the nanorings to regulate the deposition and recrystallization of small organic molecules from the liquid phase. Three hydrophobic molecules in the crystalline powder form are used for the recrystallization study: n-docosane, 2-acetoxybenzoic acid, and clarithromycin. The nanoring patterns made in 0.13 L reactor at 5% relative humidity and after 90 min reaction time on the PS900 and PS300 templates are used for nanoparticle deposition. Figure 6 shows the two patterns before filling them with the organic molecules. The nanorings made with the PS900 template are 14.4 ± 2.4 nm in height, 160 ± 32 nm in inner diameter, and 379 ± 46 nm in outer diameter. The nanorings formed on the PS300 template are 10.3 ± 2.2 nm in height, 56 ± 14 nm in inner diameter, and
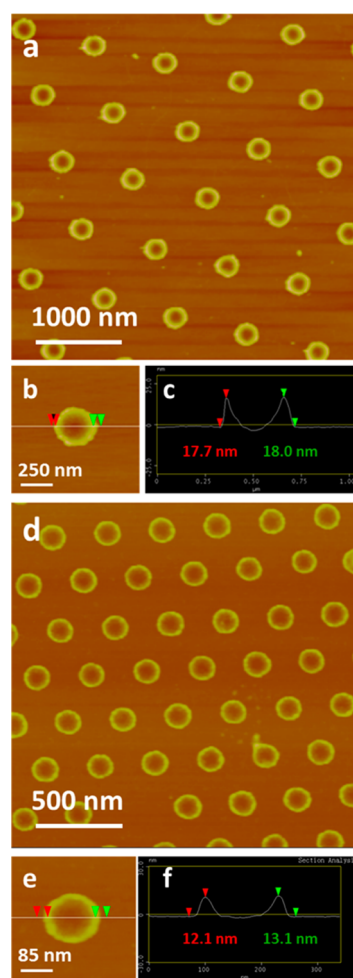

Figure 6. AFM height image data of the OTS nanorings made with the (a−c) PS900 template and (d−f) PS300 template. Z-range = 60 nm.

121 ± 25 nm in outer diameter. The AFM images and sectional height analysis show that the nanopatterns display uniform nanostructures and the nanorings are spherical in shape. If we fill all the spherical caps to the top of the nanoring pattern we expect to create 1×10^8 nanoparticles/cm^2 of uniformly distributed nanoparticles each with a fixed volume of $(3.0 \pm 1.5) \times 10^{-10}$ nL on the PS900 nanopattern and 5×10^8 nanoparticles/cm^2 of particle volume $(5.0 \pm 2.0) \times 10^{-11}$ nL on the PS300 nanopattern.

The supra-monolayer nanorings are stable against repeated solvent treatments. We have conducted AFM and contact angle measurements before and after immersing the nanopatterns in organic solvents including chloroform, diethyl ether, heptane, and 1-butanol for at least 30 min and found no evidence of pattern erosion or degradation. We have also imaged the nanopattern in 1-butanol and heptane by AFM and found no evidence of pattern swelling or degradation while immersed in the solvents. It shows that OTS molecules are polymerized to a high degree to form the nanorings.

The first compound used to fill the nanorings is *n*-docosane. *n*-Docosane is chosen as a model compound because it belongs to the *n*-alkane homologous series with known chain length dependent physical properties such as melting temperature and solubility. *n*-Docosane has a melting temperature of 43 °C. Various solvents have been used to deposit *n*-docosane films on the OTS nanopattern. Diethyl ether with the highest vaporization rate of all the solvents tested has been found to yield the smoothest *n*-docosane film. To ensure uniform particle formation, we first heated the as-deposited film above its melting temperature to yield a uniform film thickness and then is quickly cooled to −20 °C. We have been able to produce uniform particles following this procedure as well as vary the amount of *n*-docosane deposited per nanoring as a function of its concentration in diethyl ether. Little *n*-docosane is deposited when the concentration is lower than 0.7 mM. On the other hand, the deposited layer is much thicker than the nanopattern when the concentration is higher than 7 mM. At concentrations between 0.7 and 7 mM increasing amount of *n*-docosane is deposited inside the nanoring with increasing concentration (Figure 7). *n*-Docosane solidifies almost exclusively inside the nanorings in a concentration range of 0.7−3.5 mM. The average nanoparticle height is 15 nm at 1 mM and reaches the maximum value of 19 nm at 3.5 mM. At 3.5 mM the *n*-docosane volume contained per nanoring is 5−7 times the calculated cap volume indicating that *n*-docosane overfills the nanoring above the nanopattern height (= 15 nm) by the simple solidification process. After reaching the maximum filling increasing amount of *n*-docosane is deposited outside the nanoring with increasing concentration. The substrate is covered by a continuous layer of *n*-docosane at 7 mM. The uniform *n*-docosane nanoparticle size and distribution clearly demonstrates the ability of the OTS nanopattern to regulate molecular deposition and solidification of organic molecules and its potential use as "nano-flask" arrays for the manufacture of organic nanoparticles and nanoparticle arrays via the simple melt solidification route.

An alternative route to melt solidification is evaporative precipitation and crystallization of organic nanoparticles from the solution phase on the nanopattern. A 40 μL droplet of *n*-docosane, 2-acetoxybenzoic acid, or clarithromycin of various concentrations in diethyl ether is placed on the patterned substrate followed by fast evaporation of diethyl ether. The amount deposited is a function of the solution concentration.
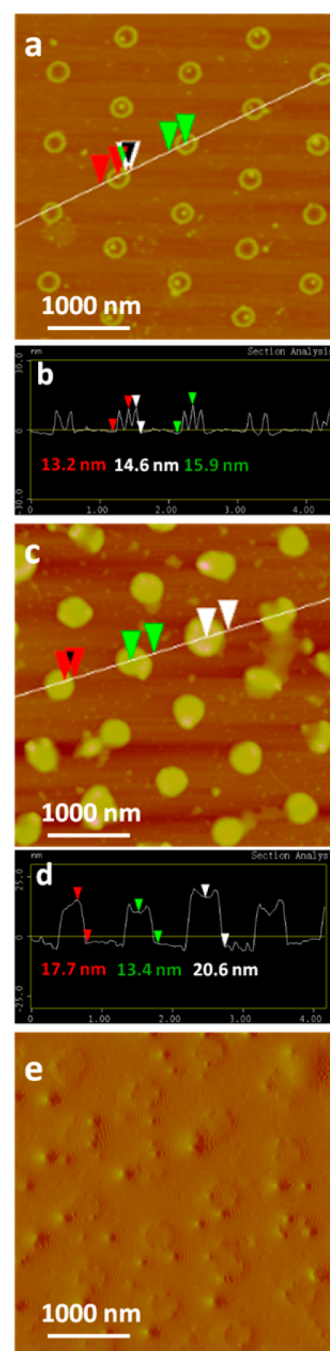

Figure 7. AFM images and sectional height analyses of *n*-docosane nanoparticles deposited on the nanoring pattern by melt solidification. The PS900 template is. The amount deposited is varied by the initial solution concentration used prior to melting of the film: (a−b) 1, (c−d) 3.5, and (e) 7 mM. Z-range for (a−d) is 60 nm. Z-range for e is 1 V (amplitude image).

Maximum filling of the nanoring occurs at 0.7, 3, and 0.2 mM for *n*-docosane, 2-acetoxybenzoic acid, and clarithromycin, respectively (see Figure S2 in the Supporting Information). Figure 8 and Figure S3 (Supporting Information) show the dependence of nanoparticle size on solution concentration in the PS300 and PS900 case, respectively. The corresponding particle volume versus concentration data are plotted in Figure 9. Figure 8d is an FESEM image of 2-acetoxybenzoic acid deposited on the nanopattern made with the PS300 template from 0.1 mM solution that matches closely the features from
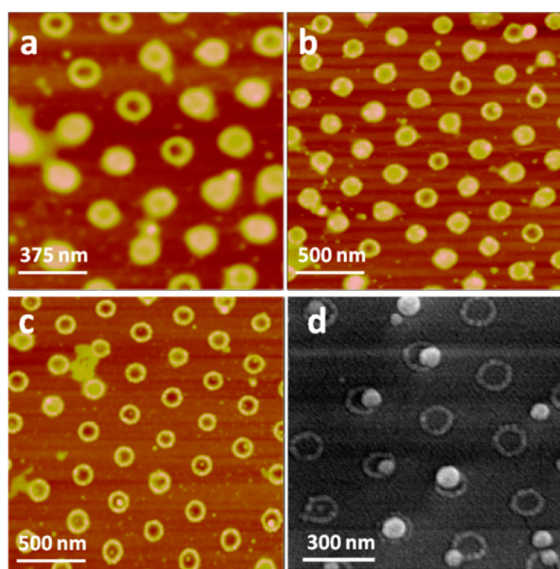
Figure 8. AFM images of 2-acetoxybenzoic acid nanoparticles deposited on the PS300 nanopattern from (a) 1, (b) 0.3, and (c) 0.1 mM solution. Z-range = 20 nm. (d) FESEM image of the c sample.
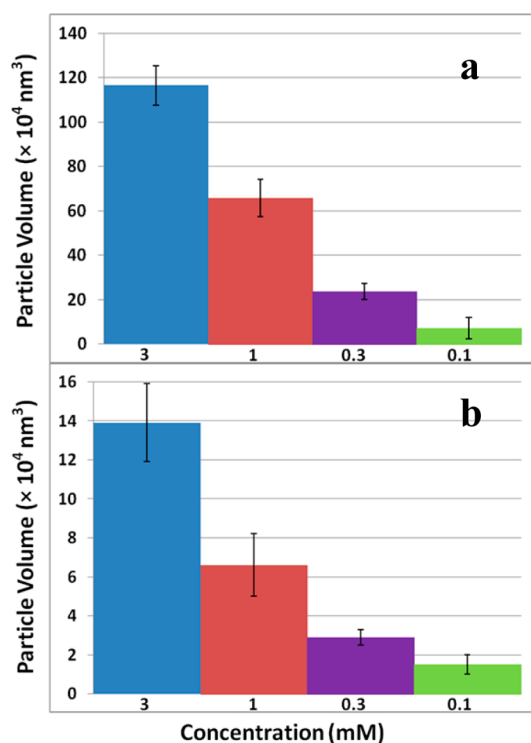

Figure 9. Dependence of 2-acetoxybenzoic acid nanoparticle volume inside the nanoring as a function of solution concentration on both (a) PS900 and (b) PS300 templates.

the AFM images. Both AFM and SEM images show that while the location of the nanoparticles inside the nanorings is not fixed, a high percentage of the nanoparticles are attached to the nanoring suggesting that the nanoring inner wall is the preferred nucleation site for the organic molecule precipitation and crystallization.

The molecular nanoparticles arrays can be transferred from the nanorings to another substrate such as an adhesive tape or a

silicone rubber stamp by pressing the substrate against the nanopattern substrate.

What is the crystalline structure of the nanoparticles deposited in the nanoring? Although we do not have the answer for this question, our preliminary FTIR investigation suggests that 2-acetoxybenzoic acid nanoparticles deposited in the nanorings are crystalline in nature. Figure 10 shows the
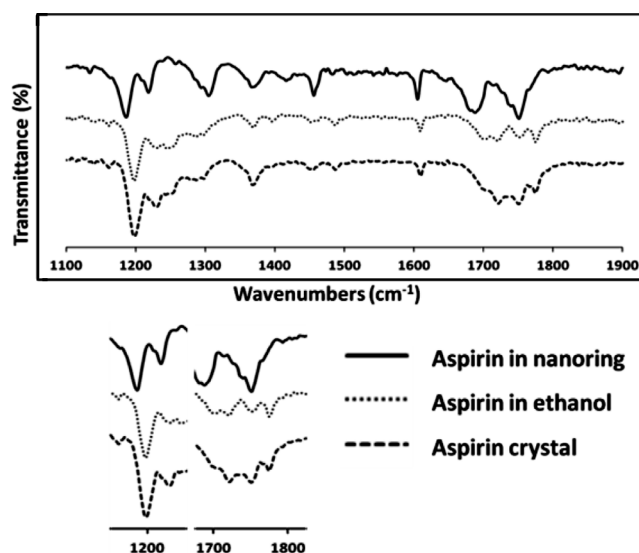

Figure 10. FTIR spectra of 2-acetoxybenzoic acid in crystalline powder, solution, and nanoparticle forms. The *y*-axis has been offset for clarity.

FTIR spectra of 2-acetoxybenzoic acid in as-purchased crystalline powder form, solution state in ethanol, and the nanoparticle form precipitated on the nanopattern, respectively. The sample at maximum filling with least deposition outside the ring is used to minimize the contribution from deposits outside the ring. The FTIR spectrum of the 2-acetoxybenzoic acid nanoparticles resembles more closely that of the crystalline powder.

Precipitation and crystallization on patterned surfaces and in mesoporous and microfluidic devices are pursued as high-throughput alternatives to the traditional manual screening of protein and small molecule drug crystallization conditions because of the rapid advances in nanomedicine and genome sequencing. ω-Terminated alkanethiol SAM micropatterns, made by microcontact printing, have been used to study $CaCO_3$ precipitation and crystallization.[36] The geometry, surface chemistry, and number of preferred nucleation sites are precisely defined by the micropattern. By making the distance between neighboring preferred nucleation sites smaller than their overlapping depletion zone calcite nucleation is confined only to the patterned area. The depletion zone is defined by the rapid molecular flux into the nucleation site that lowers the nearby concentration to below the critical nucleation concentration. In our case, rapid cooling or evaporation necessary for uniform film formation corresponds to nucleation with the smallest depletion zone. Therefore, it is unlikely that the high fidelity between the nanoparticle arrays and nanoring pattern is achieved under the same mechanism as in the case of calcite nucleation on the SAM micropattern. Instead, we propose that the preferential deposition of the organic molecules inside the nanoring below a certain concentration is due to the dewetting of the liquid film on the nanoring

template. If the substrate were to be completely immersed in the liquid during nucleation then one would expect at least some organic molecules to deposit outside the ring at these very high solidification rates. The proposed dewetting process effectively distributes the liquid film among the "nano-flasks" so that millions of solution experiments can be carried out in isolated droplets with droplet volume as small as 1×10^{-10} nL on the patterned wafer substrate. When nucleation occurs in such small volumes the number of nuclei is limited due to the large depletion zone size relative to the liquid droplet size. In fact of all the nanorings examined very few of them contain more than one nanoparticle per nanoring on either the PS300 or the PS900 pattern. The uniform particle size is achieved on the nanorings by allowing only one nucleus formation per small droplet volume. Reducing liquid droplet size to the nanometer size is also effective in eliminating the dominant role of a few contaminants in nucleation studies. There is evidence that nucleation occurs at the inner wall of the nanoring likely due to the high flux at the three-phase contact line between the liquid droplet and ring inner wall perimeter.

CONCLUSIONS

This research has determined OTS chemical vapor deposition conditions for particle lithography using polystyrene colloidal particles of 300 and 900 nm in diameter that yield nanorings with multilayer thickness. The OTS nanoring thickness varies between 14 and 23 nm with the maximum value obtained at the beginning of the reaction. The patterned substrate hydrophobicity can be further tuned by OTS reaction time. The supra-monolayer nanorings are stable against repeated solvent treatments, which make them suitable for use in organic solvents. The supra-monolayer nanorings have been used as "nano-flasks" to solidify nanoparticles of small crystalline molecules including *n*-docosane, 2-acetoxybenzoic acid, and clarithromycin. The supra-monolayer OTS nanopattern has been found to be an effective template for nanoparticle array deposition of all three chemicals with uniform particle size and spatial distribution as dictated by the OTS pattern. The particle size can be further reduced by solution concentration. The research demonstrates a particle lithographical method to manufacture supra-monolayer patterns as containers of extremely small liquid droplets and their potential use for high-throughput crystallization trials and manufacture of monodisperse organic/drug nanoparticles. The pattern can be used for the study of nanoscale topographical and chemical features on crystal nucleation. The combination of small particle size and even spatial distribution could offer a means to formulate low-dose drug delivery devices with precise dosage control.

ASSOCIATED CONTENT

Ⓢ Supporting Information

Electron microscope images of PS spheres removed from the substrate after CVD; more AFM images showing PS300/900 nanorings filled with docosane, clarithromycin, and 2-acetoxybenzoic acid; scheme of various proposed nanostructures of the nanorings. This material is available free of charge via the Internet at http://pubs.acs.org/.

AUTHOR INFORMATION

Corresponding Author

*Tel:. 313 577 3804. E-mail: gzmao@eng.wayne.edu.

Notes

The authors declare no competing financial interest.

ACKNOWLEDGMENTS

REFERENCES

(1) Sagiv, J. *J. Am. Chem. Soc.* **1980**, *102*, 92−98.

(2) Kessel, C.; Granick, S. *J. Am. Chem. Soc.* **1991**, *7*, 532−538.

(3) Dong, J.; Wang, A.; Ng, K. Y. S.; Mao, G. *Thin Solid Films* **2006**, *515*, 2116−2122.

(4) Wasserman, S. R.; Tao, Y. T.; Whitesides, G. M. *Langmuir* **1989**, *5*, 1074−1087.

(5) Wasserman, S. R.; Whitesides, G. M.; Tidswell, I. M.; Ocko, B. M.; Pershan, P. S.; Axe, J. D. *J. Am. Chem. Soc.* **1989**, *111*, 5852−5861.

(6) Ruhe, J.; Novotny, V. J.; Kanazawa, K. K.; Clarke, T.; Street, G. B. *Langmuir* **1993**, *9*, 2383−2388.

(7) Legrange, J. D.; Markham, J. L.; Kurkjian, C. R. *Langmuir* **1993**, *9*, 1749−1753.

(8) Denkov, N. D.; Velev, O. D.; Kralchevsky, P. A.; Ivanov, I. B.; Yoshimura, H.; Nagayama, K. *Langmuir* **1992**, *8*, 3183−3190.

(9) Denkov, N. D.; Velev, O. D.; Kralchevsky, P. A.; Ivanov, I. B.; Yoshimura, H.; Nagayama, K. *Nature* **1993**, *361*, 26−26.

(10) Li, J. R.; Garno, J. C. *Nano Lett.* **2008**, *8*, 1916−1922.

(11) Li, J. R.; Lusker, K. L.; Yu, J. J.; Garno, J. C. *ACS Nano* **2009**, *3*, 2023−2035.

(12) Lusker, K. L.; Yu, J. J.; Garno, J. C. *Thin Solid Films* **2011**, *519*, 5223−5229.

(13) Aizenberg, J.; Black, A. J.; Whitesides, G. M. *Nature* **1999**, *398*, 495−498.

(14) Briseno, A. L.; Mannsfeld, S. C. B.; Ling, M. M.; Liu, S. H.; Tseng, R. J.; Reese, C.; Roberts, M. E.; Yang, Y.; Wudl, F.; Bao, Z. N. *Nature* **2006**, *444*, 913−917.

(15) Cheng, W. L.; Park, N. Y.; Walter, M. T.; Hartman, M. R.; Luo, D. *Nat. Nanotechnol.* **2008**, *3*, 682−690.

(16) Courty, A.; Mermet, A.; Albouy, P. A.; Duval, E.; Pileni, M. P. *Nat. Mater.* **2005**, *4*, 395−398.

(17) Mao, G.; Chen, D.; Handa, H.; Dong, W.; Kurth, D. G.; Mohwald, H. *Langmuir* **2005**, *21*, 578−585.

(18) Mao, G.; Dong, W.; Kurth, D. G.; Mohwald, H. *Nano Lett.* **2004**, *4*, 249−252.

(19) Zhong, Z.; Gates, B.; Xia, Y.; Qin, D. *Langmuir* **2000**, *16*, 10369−10375.

(20) Dong, W.; Wang, R.; Mao, G.; Mohwald, H. *Soft Matter* **2006**, *2*, 686−692.

(21) Chen, D.; Wang, R.; Arachchige, I.; Mao, G.; Brock, S. L. *J. Am. Chem. Soc.* **2004**, *126*, 16290−16291.

(22) Wang, R.; Li, L.; Arachchige, I.; Ganguly, S.; Brock, S. L.; Mao, G. Z. *ACS Nano* **2010**, *4*, 6687−6696.

(23) Wang, S.; Li, L.; Mao, G. *J. Phys. Chem. C* **2012**, *116*, 5492−5498.

(24) Cassie, A. B. D. *Discuss. Faraday Soc.* **1948**, *3*, 11−16.

(25) Wu, B.; Mao, G.; Ng, K. Y. S. *Colloids Surf., A* **2000**, *162*, 203−213.

(26) Chen, J.; Liao, W. S.; Chen, X.; Yang, T.; Wark, S.; Son, D. H.; Batteas, J. D.; Cremer, P. S. *ACS Nano* **2009**, *3*, 173−180.

(27) Dong, J. *Thin Solid Films* **2006**, *515*, 2116−2122.

(28) Wasserman, S.; Tao, Y.; Whitesides, G. *J. Am. Chem. Soc.* **1989**, *5*, 1074−1087.

(29) Hair, M. L.; Hertl, W. *J. Phys. Chem.* **1969**, *73*, 2372−&.

(30) Angst, D. L.; Simmons, G. W. *Langmuir* **1991**, *7*, 2236−2242.

(31) Fadeev, A. Y.; McCarthy, T. J. *Langmuir* **2000**, *16*, 7268−7274.

(32) Ashurst, W. R.; Carraro, C.; Maboudian, R. *IEEE Trans. Device Mater. Reliab.* **2003**, *3*, 173−178.

(33) Ahn, W.; Roper, D. K. *ACS Nano* **2010**, *4*, 4181−4189.

(34) Takei, T.; Mukasa, K.; Kofuji, M.; Fuji, M.; Watanabe, T.; Chikazawa, M.; Kanazawa, T. *Colloid Polym. Sci.* **2000**, *278*, 475−480.

(35) Asay, D. B.; Kim, S. H. *J. Phys. Chem. B* **2005**, *109*, 16760−16763.

(36) Aizenberg, J. *Adv. Mater.* **2004**, *16*, 1295−1302.